MJO-induced Warm Pool Eastward Extension Prior to the Onset of El Niño: An Observational study

Yakelyn R. Jauregui

A dissertation
submitted in partial fulfillment of the
requirements for the degree of

Master of Science

University of Washington

2020

Reading Committee:

Shuyi S. Chen, Chair

David Battisti

Daehyun Kim

Chidong Zhang

Program Authorized to Offer Degree:
Atmospheric Sciences

University of Washington

Abstract

MJO-induced Warm Pool Eastward Extension Prior to the Onset of El Niño: An Observational study

Yakelyn R. Jauregui

Chair of the Supervisory Committee:
Professor Shuyi S. Chen
Atmospheric Sciences

The Madden-Julian Oscillation (MJO) and El Niño Southern Oscillation (ENSO) are the two most important phenomena in the Tropics that affect global weather and climate on intraseasonal to interannual timescales. Although they occur on different timescales, the MJO-induced SST changes over the western Pacific have spatial scales similar to those of SST anomalies prior and/or during the onset of El Niño. To investigate the MJO-induced SST changes and their contribution to the warm pool eastward extension (WPEE) prior to the onset of El Niño, we use 20 years of Tropical Rainfall Measuring Mission (TRMM) Multi-satellite Precipitation Analysis (TMPA), Cross Calibrated Multi-Platform (CCMP) surface winds, and Optimum Interpolated Sea Surface Temperature (OISST) to quantify the time and spatial scales of MJO rain and wind, and the MJO-induced WPEE. The MJO events in the western equatorial Pacific (east of 130°E, 10°S – 10°N) are identified based on the Large-scale Precipitation Tracking (LPT). The intensity of the MJO is measured by total rain volume and zonal surface winds averaged throughout its lifetime. It is found that the majority of the MJOs (65%) induce a WPEE up to 3000 km that can last beyond 15 days. The MJO events prior to the onset of El Niño are generally stronger in convection and winds, and produce significant WPEE beyond the annual cycle. Consecutive MJO events produce much larger WPEE prior to El Niño, which has been observed in every El Niño event from 1998-2019.

TABLE OF CONTENTS

LIST OF FIGURES

ACKNOWLEDGMENTS

I would like to thank my advisor, Professor Shuyi Chen, for giving the opportunity to work on this topic. Her support and guidance opened many opportunities that are making me a better scientist. I would like to thank the members of the "Hurricanes and Coupled Atmosphere-Ocean Systems" team at the University of Washington. Our weekly group meetings help me to stay up to date in research, improve my science communication skills, and enhance my knowledge about other topics, for which I will always be grateful. A special thank you goes to Brandon Kerns for his help on MJO-LPT analysis and to Ajda for help on coding related matter. I also would like to thank my committee members, David Battisti, Daehyun Kim, and Chidong Zhang, for their thoughtful comments and suggestions that improved this work. Finally, I thank all the staff at the Department of Atmospheric Sciences, especially Erica Coleman.

This research is supported by a fellowship from FONDECYT – Perú and the NOAA CVP research grant NA18OAR4310401.

DEDICATION

To my family, friends, and Jorge for their support and encouragement.

Chapter 1

INTRODUCTION

1.1 Background and Literature review

1.1.1 The west-Pacific Warm Pool

The western Pacific warm pool is a considerable heat reservoir [67], a significant source of moisture for the atmosphere [12], and drives large scale circulations (the Walker circulation, Gill 1980). The spatial surface extension is usually delineated with 28°C, 28.5°C or 29°C [46, 18, 19, 65] because it delineates an area exceeding a threshold for intense convective activity [22, 68, 20]. Using 28.5°C, the long-term tropical warm pool eastern edge extends to 180° at the equator, 175°W in the north, and 150°W in the south (Figure 1a). Peculiar ocean vertical structure also characterizes the warm pool, the 28.5°C isotherm can extend up to 100m at about 170°E (Figure 1.1b). In addition, high precipitation rates, and light winds often induces a sea surface salinity (SSS) lower than 35 practical salinity units (PSU, Figure 1.1b), and result in the formation of a relatively low density and stable oceanic mixed layer [39, 67, 12]. In Figure 1.1, places where the isohaline layer is shallower than the isothermal layer, is known as a Barrier Layer (BL), in such cases, the mixed layer depth is controlled by the salinity stratification [13, 39]. At the equator, warm and fresh waters are separated from the cold and saltier waters in the central pacific by a sharp salinity front which is also characterized by a current convergence [53, 18]. The SSS front, characterized as 34.8 PSU [14, 54, 44, 10], is usually located inside the warm pool and west of the warm pool eastern edge as shown in Figure 1.1b, and its longitudinal location varies consistently with the warm pool eastern edge displacement [53, 14, 44].

1.1.2 El Niño – Southern Oscillation (ENSO)

ENSO is a coupled ocean-atmosphere phenomenon. It is the largest source of interannual variability in the tropics that impacts the Earth's climate variability through atmospheric

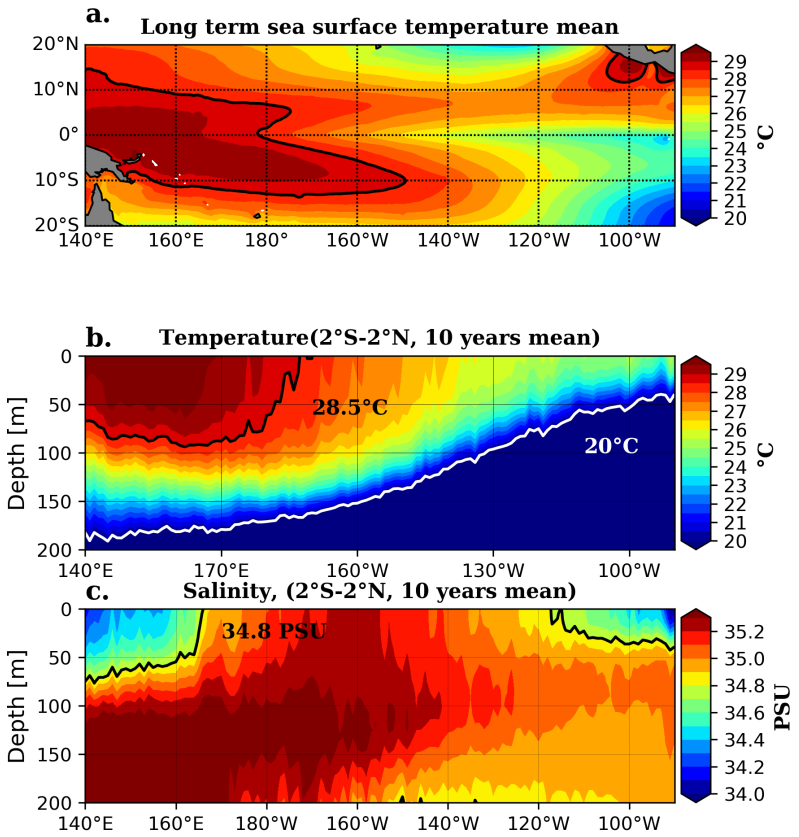

Figure 1.1: (a) Long term (30 years, OISST v2) of sea surface temperature values, the warm pool as 28.5°C in black contour. Vertical cross section at the equator (2°S-2°N) averaged over 10 years from Argo floats for (b) Temperature and (c) Salinity.

teleconnections[8, 9, 56]. It is characterized as warm or cold SST anomalies in the central and/or eastern Pacific [16], and a modified zonal slope of the thermocline along the equator [68] that result in significant changes in the zonal wind intensity [3], and location of convection areas [59]. It occurs every few years (3-5 years) and involves a positive ocean-atmosphere feedback hypothesized by Bjerknes (1969). According to Bjerknes, easterly trade winds, blowing along the equator, result in a thermocline that is deep in the west and shallow in the east (white contour in Figure 1.1b). The trade winds induce poleward Ekman divergence and upwelling that causes the SST to be cooler in the east than in the west. The horizontal temperature gradient creates a gradient in pressure that strengthens

the trade winds, which through upwelling, feedback to the SST zonal gradient, maintaining the "normal" conditions. If trade winds strengthen, the same feedback leads to La Niña conditions. On the other hand, during El Niño, the feedback leads to weaker trade winds, shallower thermocline in the west, and reduced SST zonal gradient. Theoretical understanding of ENSO properties including its amplitude, frequency, and propagating features and its changes at decadal to interdecadal timescales has significantly advanced over the past decades [66, 5]. One of the most common theoretical explanation of ENSO mechanisms holds it to be a self-sustained and naturally oscillatory mode with a period that depends on the dynamical adjustment of the subsurface ocean [60, 4]. Another explanation considers ENSO a stable mode triggered by stochastic forcing such as westerly wind bursts (WWBs), e.g. MJO events [31]. ENSO simulation and prediction in terms of large-scale ocean-atmosphere characteristics has improved; however, questions about the transition phase from one to another ENSO state remain to be answered.

1.1.3 The Madden Julian Oscillation (MJO)

The MJO is considered a wavelike phenomenon with periods ranging from 30 – 90 days. It consists of a multi-scale convective structures over thousands of kilometers near the equator that propagates eastward at an average speed of $5ms^{-1}$ [40, 41, 71]. The MJO convective signal generally initiates over the Indian Ocean, propagates through the Maritime Continent and dies over colder waters in the Pacific Ocean. Individual mesoscale convective systems often propagate westward, but with each new system forming to the east of the previous one. The propagation speed of the MJO varies, is slower when the convection and large-scale circulation are coupled together, and faster after the convection dies. The MJO exhibits a strong seasonal cycle with a strong peak in the Northern Hemisphere winter (related to the Australian Monsoon), and a weaker peak in Northern Hemisphere summer (related to the Asian Monsoon; [71]). As the active MJO propagates across ocean, the associated westerly surface winds, extensive cloud cover, and large amounts of precipitation help induce upper ocean mixing and cool the ocean surface [61]. During its propagation, fresh-water input from precipitation changes upper-ocean salinity structure [21, 39, 1]. In addition, the westerly

winds associated with the MJO excite oceanic downwelling equatorial Kelvin waves that propagate eastward across the basin in 1-2 months, affecting sea level, upper-ocean currents and temperature structures along the way [33, 27].

1.1.4 MJO and the El Niño onset

Observational evidence suggests that El Niño may require an initial surface and subsurface warming across the Pacific [31]. This initial warming is named the onset of El Niño in the central Pacific and is observed as a warm pool eastward extension (WPEE) far beyond its climatological position. It has been proposed that MJO effects on the Pacific SST contribute to the ENSO variability, particularly to the development of El Niño. This contribution has been suggested based on the MJO plausible physical mechanisms to warm the SST in the central and eastern Pacific through local and remote response to the dynamic and thermodynamic mechanisms [33, 50, 32, 6, 72, 38, 25, 10]. The physical mechanisms through which the MJO induces warming, observed as a warm pool eastward extension (WPEE), involve different processes that occur during its propagation, and after the convective signal its gone. The two main mechanisms were provided in two different studies. Kessler et al. (1995) pointed out the role of the ocean Kelvin wave forced by the MJO-induced westerly wind bursts (WWB). The ocean Kelvin wave deepens the thermocline during its propagation, decreasing the basin-scale zonal upper ocean temperature gradient, enabling the advection of warm waters to the east. This dynamic ocean response to MJO-westerlies is enhanced if consecutive MJO events occur. Then, Anderson et al. (1996), based on observational data gathered during TOGA-COARE, highlighted the importance of the MJO-induced upper ocean stratification that occurs in a sequence of steps. First, the WWB induce a strong upper-ocean mixing, and the Mixed Layer (ML) depth increases. Second, the MJO-rainfall reduces the density of the ocean surface, stratifying the upper ocean, and building up a thermal layer called Barrier Layer (BL). The last stage exists if the ocean stratification remains and after the MJO convective signal (e.g., under a weak wind regime and clear skies). The shallow ML allows maximum warming by capturing a significant portion of the shortwave radiation, especially under the presence of a thick BL that serves as an important

blockade that prevents the cold thermocline water from entering the ML. A shallow ML and a thick BL have significant impact on the upper mixed layer heat content and maintenance of warm temperatures confined to the surface [62, 43]. Kessler et al. (1995) provided an essential mechanism for theories that explain ENSO in terms of ocean dynamics alone, while Anderson et al. (1996) pointed out the role of ocean stratification that maintains warm SST, allowing stronger feedbacks between the atmosphere and the ocean. Together these mechanisms act to reduce the east-west temperature gradient, e.g. [32], that allows a further shift of the warm pool eastward at the onset of El Niño [46, 37]. The MJO impact on the upper ocean dynamics and thermodynamics favors the WPEE and maintenance of warm SSTs that could last from several days to weeks. Previous studies have suggested that these shorter timescale impact of the MJO on the upper ocean could contribute to El Niño onset [33, 32, 6]; however, the evolution from an early stage to a developed El Niño phase depends on favorably ocean dynamics, in conjunction with air-sea interactions to strengthen and prolong the SST warming [68, 50, 6, 31, 5].

1.2 Science objectives

Although the MJO-induced WPEE implication to El Niño has been suggested, e.g. [33, 1, 32, 6], it has never been quantified based on long-term observations. The purpose of this study is to do so using unprecedented 20 years of satellite data to quantify the extent and duration of the MJO-induced WPEE for individual and consecutive MJO events in relation to the onset of the six El Niño events that occurred from 1998 – 2019. This study addresses the following science questions.

- How much WPEE is induced by the MJO?
- How does the MJO-induced WPEE relate to El Niño?

1.3 Outline

We present our methodology and data in Chapter 2 and the results is structured in five sections in Chapter 3: Section 3.1 describes two cases of MJO enhanced activity followed by

a WPEE. Section 3.2 summarize the MJO and ENSO lagged observed relationship during 1998-2019. Section 3.3 characterize the post-MJO WPEE in time and space, describes the annual cycle of the MJO and the MJO-induced WPEE. Section 3.4 examine the MJO intensity in relation to the WPEE emphasizing the MJO group effort in moving the warm pool eastward. Finally, Section 3.5 examines the extent of the warm pool displacement in relation to the MJO intensity of convection and westerly winds, and quantify the MJO-induced SST warming using composite analysis. Chapter 4 summarizes the main results and conclusions.

Chapter 2

DATA AND METHODS

2.1 Data

To characterize MJO events, we use precipitation from the Tropical Rainfall Measuring Mission (TRMM) Multi-satellite Precipitation Analysis (TMPA) that provides estimates of instantaneous rain rates at 3-hourly on a regular 0.25° grid based on passive-microwave and infrared retrievals [28]. Additionally, we use 6-hourly 10 m wind vector data from the Cross-Calibrated Multi-Platform version 2 (CCMP V2) gridded surface vector produced by Remote Sensing Systems (REMSS) [2]. CCMP V2 combines winds data from Version-7 REMSS radiometer, QuikSCAT, and ASCAT scatterometers, moored buoy, and ERA-Interim model using a Variational Analysis Method. To document the SST spatial evolution, we use daily SST data obtained from the National Ocean Atmospheric Administration (NOAA) Optimum Interpolation Sea Surface Temperature version 2 (OISST v2) [57, 58] at 0.25° spatial resolution. The Niño 3.4 (5°S-5°N, 170°E-120°W) SST monthly anomalies are obtained from the NOAA Earth Sciences Research Laboratory. We examine data from 1998/06 to 2019/06.

2.2 MJO identification

The MJO events are identified based on the large-scale precipitation tracking (LPT) algorithm developed and described in [30] using TRMM -GPM satellite data. Kerns and Chen (2019) provides a detailed description and statistics of MJO events occurred from 1998/06 to 2018/06, but our database is extended to 2019/06 using the same methodology. The LPT uses spatially smoothed 3-day rainfall accumulation first to identify and then to track precipitation features called Large-scale precipitation objects (LPO). An LPO must be at a large-enough scale of at least 1000 km^2; it encloses an area over which the 3-day accumulated rainfall exceeds 12mm. LPOs connected in time for at least 7 days (10 days,

including the accumulation period) constitute an MJO event if they propagate eastward. This method identifies the evolution of individual MJO events in both time and space that is not possible when using other indices. Besides, a time-filtering is not required to construct an individual MJO event; thus, its usage can be more practical to asses weather impacts and ENSO forecasts.

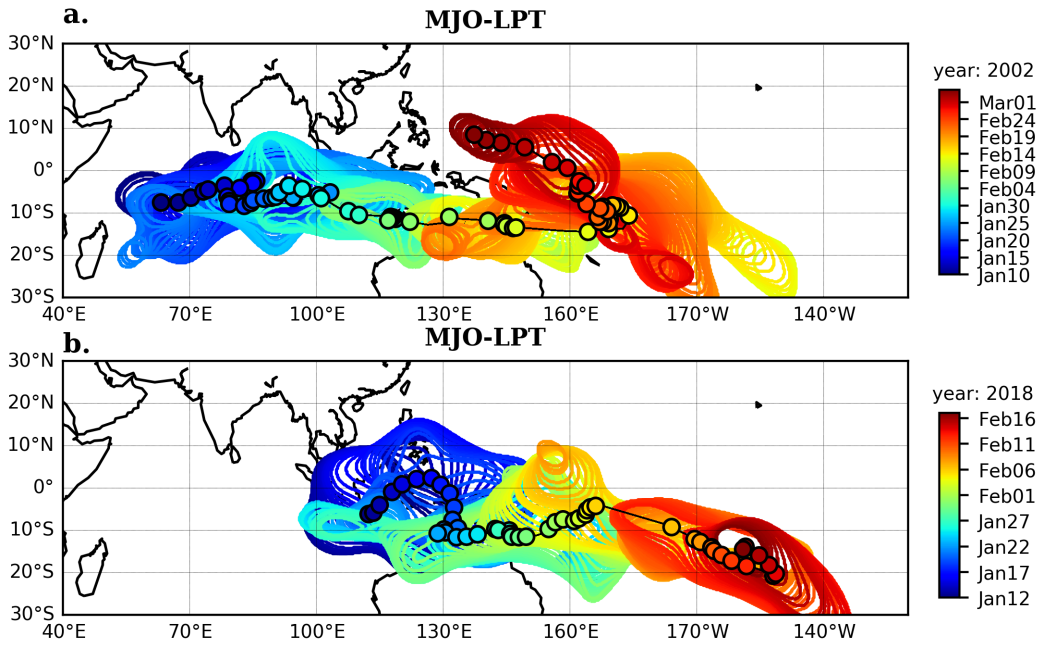

Figure 2.1: The 3 hourly MJO-LPT feature contour and their corresponding centroid drawn every day with dates according to the color scale on the right for an event in 2002 and another in 2018.

Figure 2.1a and b illustrate the evolution of two MJO events identified by the LPT method. The colors indicate time progression, while the contours outline LPOs, the markers indicate centroids of each contour. Each MJO event has parameters such as the initial and ending date, initial and ending centroid longitude, and initial and ending latitude. The MJO in 2002 starts on January 10 in the Indian Ocean and ends on March 5 in the western Pacific, its lifetime is about 50 days with an eastward speed of $1.7ms^{-1}$. The MJO in 2018 starts on January 12 and ends on February 18, with a lifetime of about 36 days and an eastward speed of 3.1 ms^{-1}. To examine the MJO impact on the warm pool, we only include MJO events with starting longitude west of 180°E and ending longitude east of

130°E. Besides, each MJO has to last at least 10 days in the western Pacific (east of 130°E), with latitude centroids located between 10°S and 10°N. A total of 98 MJO events from 1998/06 to 2019/06 are identified based on these criteria.

2.3 MJO intensity

The MJO, by definition, is characterized as large-scale convection and circulation [42, 71]. The MJO convective signal includes a multiscale cloud system known as the "active phase," surrounded both east and west by regions of weak deep convection and precipitation, known as the "suppressed phase." On the surface, strong WWB are observed in and to the west of the active phase and strong easterly winds to the east in the suppressed phase [71]. Both the WWB and rain rates are essential to characterize the MJO intensity because they exert a robust thermodynamic and dynamic control on the upper ocean. The MJO intensity in the western Pacific varies during its propagation, it could shift south towards the SPCZ or north towards ITCZ.

We define the intensity of convection and westerly winds as the accumulated 3-hourly rain rates (in mm) and 6-hourly averaged surface westerly winds (in ms^{-1}) inside each LPO. Then, the rain rates are accumulated and the WWBs are averaged throughout the lifetime of each MJO-LPT system (shading colors in Figure 2.2). The MJO envelope (purple contour in Figure 2.2) indicates the area encompassed by the MJO-LPT feature smoothed with to a 2.5° latitude/longitude Gaussian for the MJO events illustrated in Figure 2.1. The region 130°E-180°E and 10°S-10°N represents the area of MJO impact on the warm pool (WPbox, in red Figure 2.2). Then, the MJO intensity of convection over the warm pool is defined as the rain integrated over the overlapping region between the MJO envelope and the WPbox (Rain Volume in km^3). Similarly, the intensity of WWB is the average over the same region in ms^{-1}. Thus, each MJO intensity is quantified in terms of Rain Volume and WWB. Different regions were tested (140°E-180°E, 15°S – 15°N, 130°E-180°E, 15°S – 15°N) and we obtained similar results and conclusions.

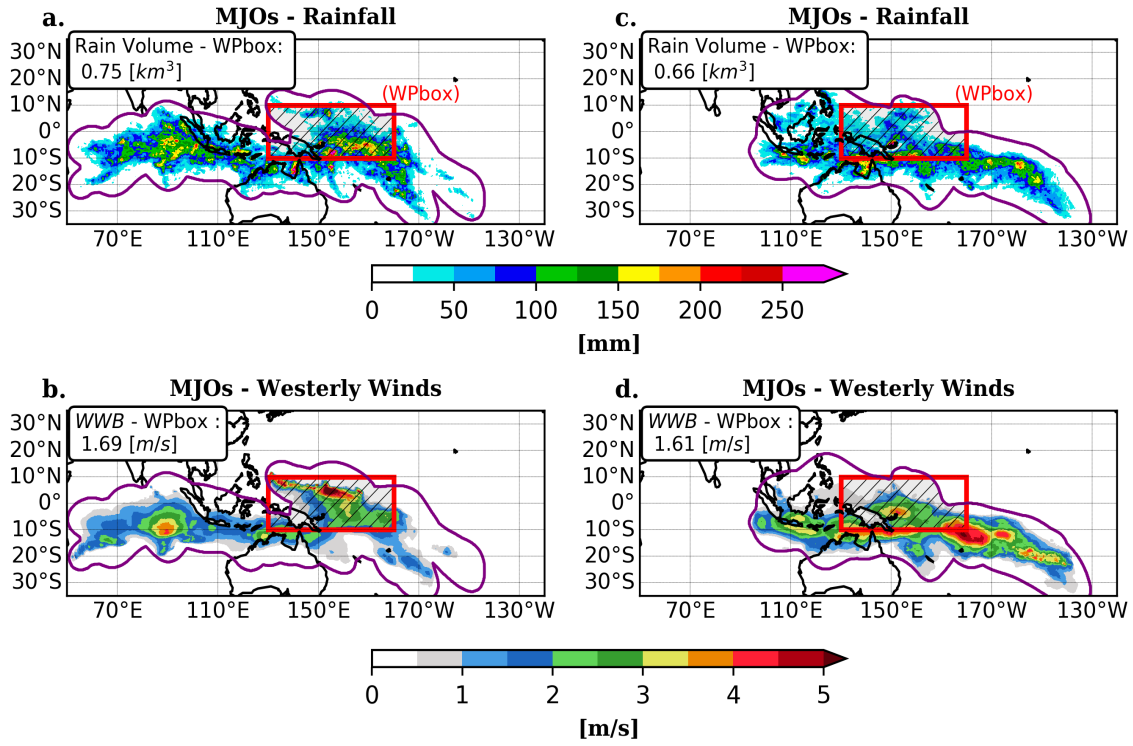

Figure 2.2: The MJO envelope (purple contour) indicates the area encompassed by the MJO-LPT feature. The red box indicates the region of MJO impact on the Warm Pool (WPbox, 130°E-180°E, 10°S – 10°N). (a) and (c) Accumulated rainfall every 3-hours, (b) and (d) Westerly winds averaged every 6-hours inside the MJO-LPT feature throughout the MJO lifetime. Units of rainfall is mm, and westerly winds is ms^{-1}. The top-left box in (a) and (c) shown the integrated rainfall (Rain Volume in m3) within the overlapped area between WPbox and the MJO envelope (hatched). The top-left box in (b) and (d) shows the average of westerly winds (WWB in ms^{-1}) within the overlapped area between WPbox and the MJO envelope (hatched).

2.4 Post-MJO warm pool eastward extension (WPEE)

The precise definition of the warm pool varies but is often delineated by the 28°C, 28.5°C or 29°C isotherms when studying the equatorial eastern edge of the warm pool, and its relevance for ENSO dynamics [55, 11, 46, 54]. We tested different isotherms; the 28°C loosely defines only one area in the west Pacific. The 29°C isotherm delineates smaller and broken areas making it difficult to track only one contour per day. Thus, we used 28.5°C

isotherm as a proxy of the warm pool. The high-frequency variability was excluded using a 3-day centered SST moving mean and a two-dimensional Gaussian smoother with a standard deviation of 10 grid points (2.5°, approximately 250km near the equator). To facilitate the analysis of the warm pool evolution post-MJO events, Day-0 (D0) refers to the MJO-LPT ending date and Day-1 to the following day. Then, the warm pool spatial structure is tracked for each day after the MJO event until it reaches a maximum eastward displacement (see Section 2.2.1 for details), as illustrated in Figure 2.3. The warm pool extends eastward up to 37 days and up to 77 days after the MJO events illustrated in Figure 2.1. In addition, we define the equatorial warm pool (EqWP hereafter) as the longitude of the 28.5°C in the 3-day centered mean SST averaged from 5°S to 5°N.

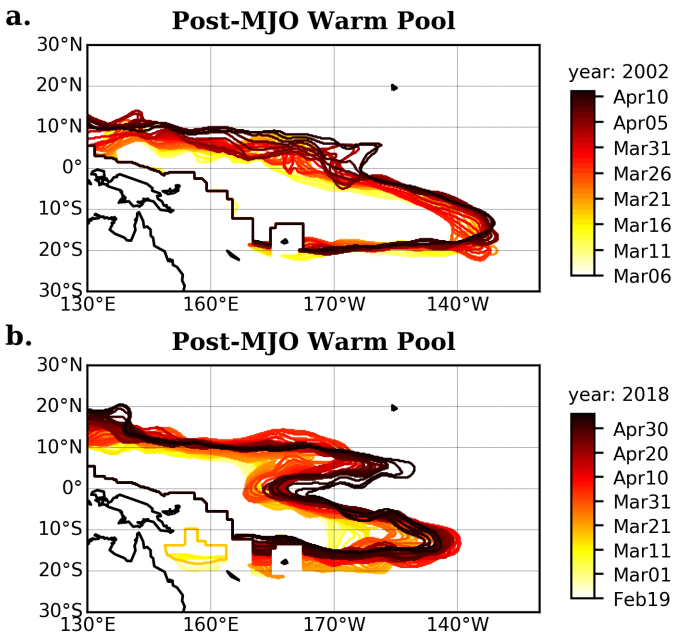

Figure 2.3: The Warm Pool after MJO events illustrated in Figure 2.1 with dates according to the color scale on the right.

2.5 WPEE quantification

The warm pool displacement is quantified as the difference of the warm pool longitude at each day post-MJO, relative to the longitude at Day-0 (D0), from 10°S to 10°N, every 0.25°.

Top panels in Figure 2.4 show the warm pool displacement up to 100 days post-MJO for the events illustrated in Figure 2.1. The bottom panels in Figure 2.4 show the equatorial band (5°S - 5°N) averaged displacement for each day post-MJO. A 5-day centered mean is applied to remove high-frequency variability and to track only the large-scale warm pool displacement. The equatorial band of the warm pool displacement is tracked in time until it reaches the maximum WPEE (Max-WPEE) that occurs at Day-Max (Dmax), allowing short ($< 500km$) and temporary (< 7 days) retreats. The maximum westward displacement was computed using the same method but tracking the westward displacement. The WPEE associated with MJO events in Figure 2.1 is shown in Figure 2. Strikingly, the most significative continuous eastward displacement ($> 5000\ km$) is observed north and off the equator, close to the Intertropical Convergence Zone (ITCZ) region, in both cases.

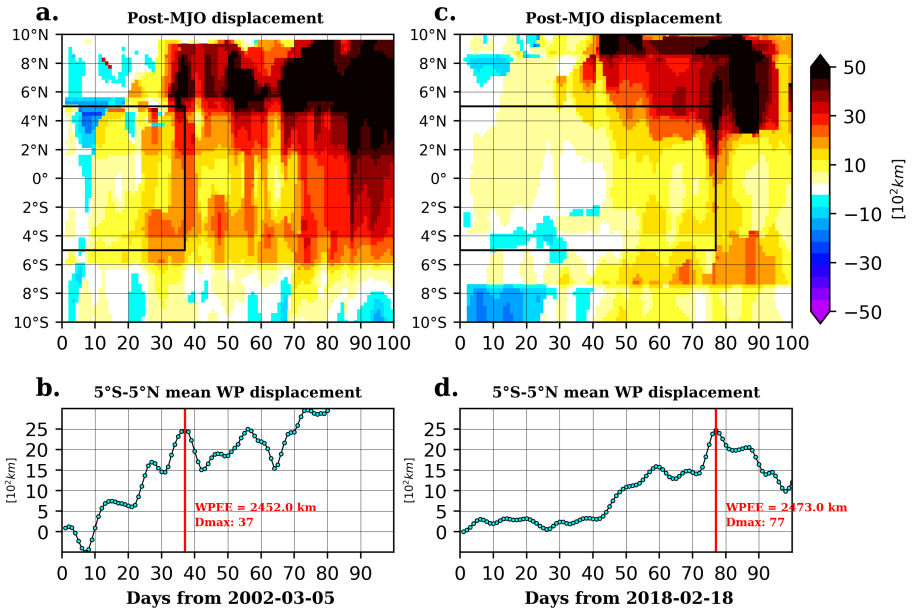

Figure 2.4: **Top panels**: The warm pool displacement relative to 2002-03-05 and 2018-02-18, respectively, for each day (x: axis) from 10°S to 10°N, every 0.25°. Color scale on the right indicate displacement in km, and black box correspond to 5°S to 5°N from Day-0 (D0) until Day-Max (Dmax). **Bottom panels**: The 5°S to 5°N averaged warm pool displacement, vertical line indicates Dmax, and Max WPEE shows the maximum eastward displacement associated with MJO events illustrated in Figure 2.1.

2.6 WPEE anomaly

The warm pool evolution and the extent of eastward displacement estimation uses absolute values of SST because it is more critical than anomalies in activating convection [22, 29], especially in the transition from the typically stable regime over the equatorial tongue to the deep convective regime. To examine whether the displacement is primarily associated with MJO events or resulting from the annual cycle we computed the warm pool anomaly (WPA) as follows. First, the warm pool daily climatology is the 28.5°C isotherm obtained from the daily SST climatology that only retains the first three harmonics of the annual cycle from 1982 – 2010, monthly values are illustrated in Figure 2.5. Then, WPA is computed by removing the daily warm pool longitude from its daily climatology longitude, from 10°S to 10°N, every 0.25°. The WPA at Dmax associated with the MJO events shown in Figure 2.1 is illustrated in Figure 2.6. In both cases, the WPA is about 3,000km close to the equator; however, more significant anomalies are observed off and north of the equator. In contrast, negative WPA is observed in the south, of about 500km and 1,500km, for each case, respectively. The WPA is computed at day D0 and Dmax for the 63 events examined in this study.

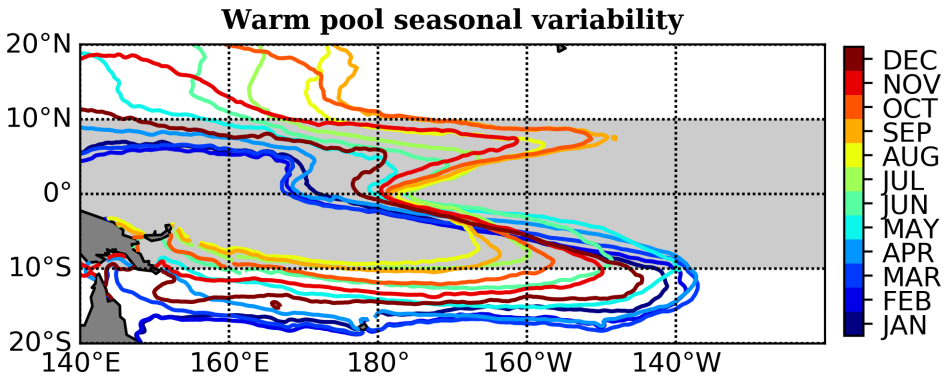

Figure 2.5: Monthly climatology (colors) of the Pacific Warm Pool (28.5°C) estimated from daily OISST from the period 1982-2010, using the first 3 harmonics of the annual cycle.

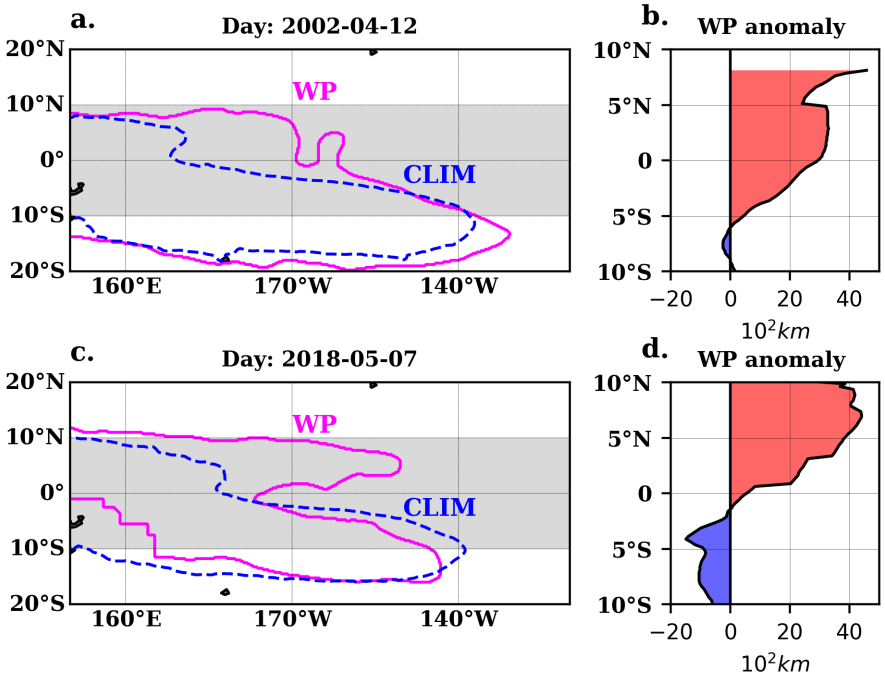

Figure 2.6: Illustration of the warm pool anomaly (WPA) at Day-Max for MJO events illustrated in Figure 2.1. The Warm Pool (WP) in magenta at its climatology (CLIM) in blue. The WPA computed as a difference of the warm pool absolute longitude relative to its climatology longitude from 10°S to 10°N every 0.25°.

Chapter 3

RESULTS

3.1 The MJO-induced WPEE before the El Niño onset

This section illustrates the WPEE that occurs after enhanced MJO activity before the onset of El Niño 2018/19 and 2002/03. Time – longitude diagrams of the equatorial averaged rain, zonal surface wind, SST and monthly Niño 3.4 values during 2018 is shown in Figure 3.1. The MJO-LPT centroids for MJOs 93-95 are shown in black contours. The passage of MJO events can be seen as three distinct convective envelopes propagating eastward at an average speed of $2ms^{-1}$. Each envelope is preceded and succeeded by weak rainfall. In contrast, the MJO passage is associated with heavy rainfall, strong and long-lasting westerly winds ($10ms^{-1}$, 15 - 30 days), and surface cooling of about 1.5° likely associated with strong upper ocean mixing and cloud cover [71, 15]. After the MJO-94 passage, under conditions of weak winds and low rain rates, the SST west of 160°E gradually increase during April and reaches 30°C by the end of the month. Then, the passage of the MJO-95 induced surface cooling but not as pronounced as for the previous events.

The most pronounced SST warming is observed after the three MJO events with values of about 30°C between 140°E - 160°E during June. This warming is possibly related to a weak convective activity and solar heating, as proposed by [1]. The Niño 3.4 region transition from cold to warm anomalies in June when the warm pool extends noticeably eastward in about 10 degrees (Figure 7d), and the large-scale east-west SST gradient and the trade winds weakened. This initial warming in the central Pacific has been highlighted by previous studies [7, 31] because it triggers deep convection and further westerly winds bursts that could move the warm pool further eastward. Indeed, convection and westerly winds at much shorter spatial and time scales than the MJO are observed during July, as the warm pool continuously moves eastward, leading to the El Niño 2018-2019, officially declared in October 2018.

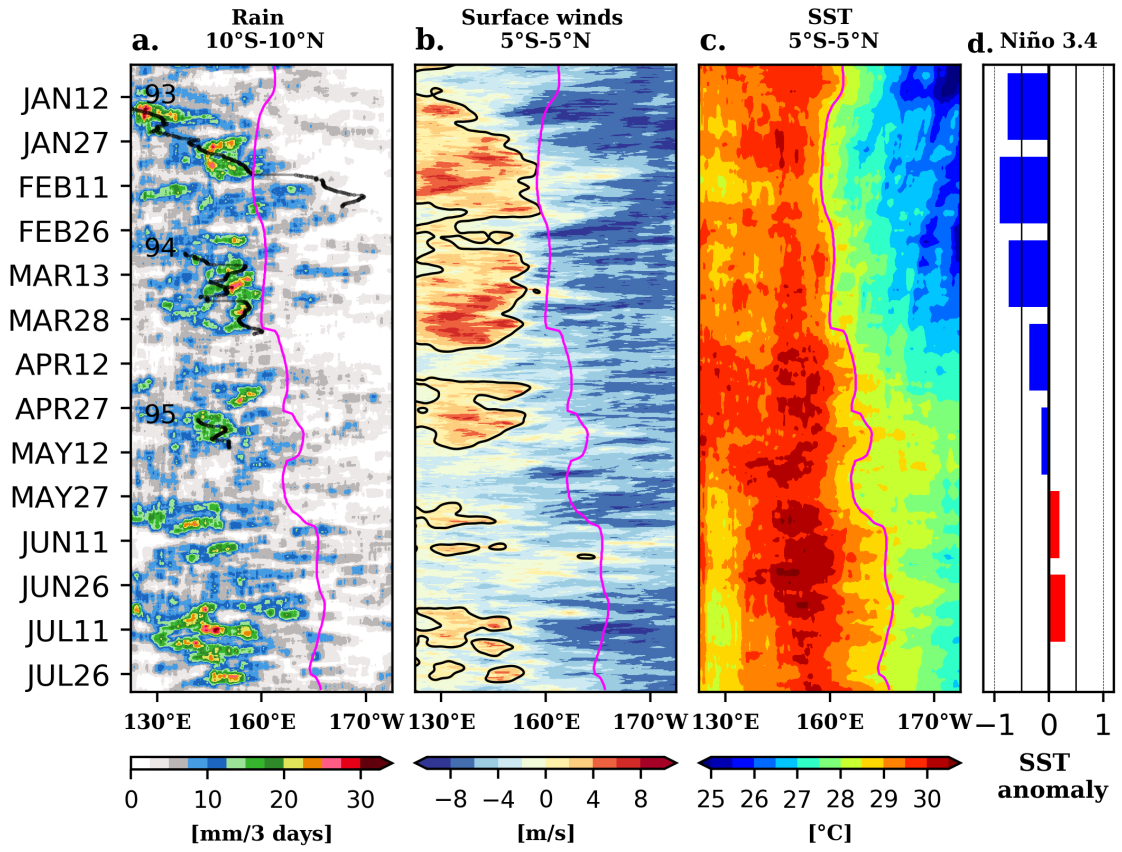

Figure 3.1: Evolution of (a) 10°S – 10°N averaged 3-day accumulated rainfall (b) 5°S-5°N averaged 6-hourly absolute zonal winds, (c) 5° S-5° N averaged SST (d) Niño 3.4 SST monthly anomalies. The equatorial warm pool (EqWP) in magenta and MJO-LPT centroids for the events 93, 94, and 95 are overlaid on each panel.

Another way to see the WPEE is by looking at SST anomalies. The evolution of SST anomalies in 2002 (Figure 3.2) shows that the large spatial scale of the MJO-induced SST anomalies resembles the spatial scale during the developing phase of El Niño 2002 (Figure 8e); however, it occurs at much shorter time scale (e.g., weeks). The MJO-induced cooling in the far western equatorial Pacific and warming in the central and eastern Pacific indicates the east-west temperature gradient and weakens the trade winds between 160°E – 140°W (Figure 8a and b), which in turn reverse at the onset of El Niño (Figure 8c). These examples suggest that the short timescale MJO effect on the surface and subsurface temperatures and

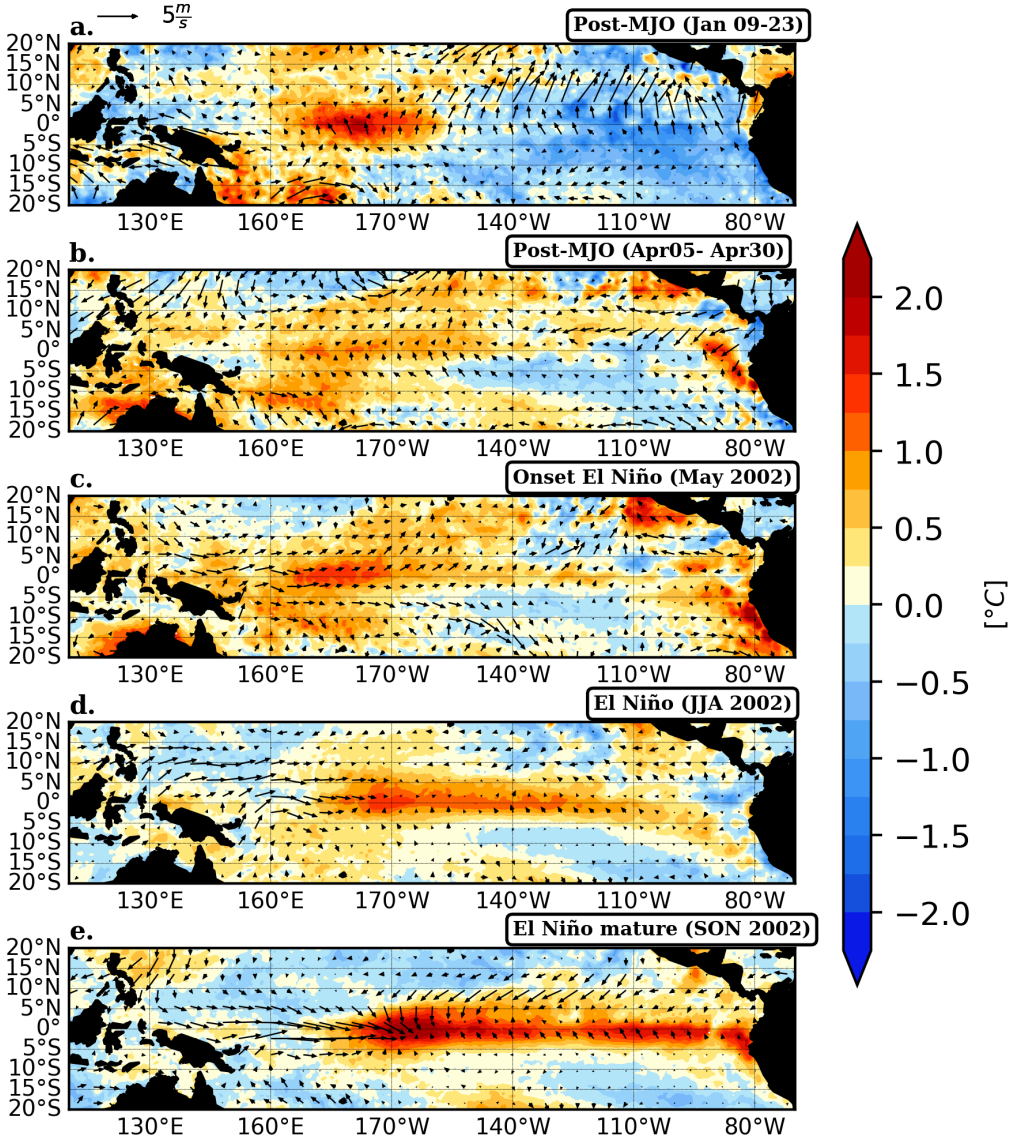

Figure 3.2: Surface winds (vectors, in m/s) and SST anomaly (color, in °C) (a) post-MJO 9-23 January 2002, (b) post-MJO 5-30 April 2000, (c) during the onset of El Niño in May 2002, (d) early stage of El Niño in June-August 2002, and (e) mature stage of El Niño in September-November 2002.

winds act as a triggering mechanism that contributes to El Niño event in the central Pacific, as also suggested by previous work [33, 32]. This work don't address the MJO contribution to El Niño but address the following question: do we observe a WPEE after each MJO

event¿

3.2 MJO and ENSO from 1998 – 2019

To better understand the MJO activity in relation to the warm pool displacement, and the onset of El Niño events, we examine events during 1998 – 2019 shown in Figure 3.3. There are six El Niño and five La Niña events during the 20 years of study. The NOAA declare El Niño advisory when Niño 3.4 exceeds 0.5°C five consecutive overlapping three-month seasons, the first three-month season characterizes the onset of each El Niño in this study. These onset months are centered on June 2002, August 2004, September 2006, July 2009, October 2014, and October 2018. To examine MJO events that could potentially contribute to the onset of El Niño, we located events that occurred within 9 months before the onset. This window chosen comes [34] that found a robust 9-month lag correlation between precursors for the onset of El Niño (e.g., equatorial sea level, zonal mean thermocline) and the Niño 3.4 index. Besides, building up conditions from cold to warm anomalies requires a high frequency forcing that can be projected on the low frequency [48, 49, 70, 45]. Enhanced MJO activity followed by a WPEE is observed before each onset of El Niño event (Figure 3.3) consistent with the MJO – ENSO lagged correlations described in previous studies [64, 32, 7, 26]. During El Niño, the already eastward extended warm pool often promotes strong MJO activity in the central Pacific; however, this study does not include MJO events that started east of 180°E. On the other hand, a contracted warm pool is associated with reduced MJO activity during a strong and long-lasting La Niña events (e.g., 1999 – 2000).

Although visual relationships between a warm pool location, MJO activity and ENSO conditions are quickly drawn from Figure 3.3, our methods identified and quantified 63 MJO-induced WPEE events. 23 MJO events occur before the El Niño onset, and the majority (19 events highlighted in red in Figure 3.3) are followed by a WPEE leading to each El Niño event. Only 4 MJO events are associated with a warm pool retreat (MJO-ids: 38, 52, 53, 78), likely associated with unfavorable large-scale atmospheric and oceanic conditions. There are 33 MJO events during El Niño (highlighted in dark red in Figure 3.3); from them, only 17 are associated with a WPEE. We first focus on the characterization of

the spatial and temporal scales of the 63 post-MJO WPEE events, and then we separate them in three groups to account for different underlying conditions (e.g., equatorial zonal wind relaxation during El Niño). One group takes into account only events before the El Niño onset, another group includes only events during El Niño, and the last group contains only non-El Niño related events that accounts neutral and La Niña conditions.

3.3 MJO-induced WPEE characterization

We characterize the MJO-induced WPEE using the information of the equatorial band (5°S-5°N) from Day-0 to Day-Max for 63 events. Generally, an eastward displacement is more common, especially during the first 15 days; but some westward displacement also occurs (Figure 3.4a). The most frequent WPEE occurs during the first 15 days with displacements up to 1,000km (Figure 3.4b). Taking this spatial and temporal scales, the WPEE speed obtained is about $0.8ms^{-1}$, which is close to the eastward Yoshida jet ($1ms^{-1}$) [69], but slower than ocean Kelvin waves ($2ms^{-1}$). Besides, less often, but significant WPEE occurs beyond 2,000km after 25 days (Figure 10a and c). The number of MJO events that produced WPEE vary from 80% (50/63) during the first 15 days to 40% that can sustain a WPEE after 25 days (Figure 3.4c).

3.3.1 Annual cycles of the MJO and MJO-induced WPEE

The MJO events with an associated WPEE have a pronounced seasonal cycle (Figure 3.5a), they are more frequent during boreal winter (21 events) and spring (26 events), shifting towards the South Pacific Convergence Zone (SPCZ). Weaker MJO activity occurs in summer (12 events) and fall (7 events) with centers of convection shifting towards the northern hemisphere, when the Asian monsoon is active. During spring, the MJO convective activity is also weak and coincides with the weakest mean equatorial zonal SST gradient along the equator [63, 26]. Likewise, the EqWP has a pronounced annual cycle; it migrates from 170°E to 170°W from boreal Spring to Summer (Figure 3.5b). However, the post-MJO WPEE equatorial warm pool is located far beyond the climatology position, especially from February to June (Figure 11b). Some consecutive MJO events are associated with the same

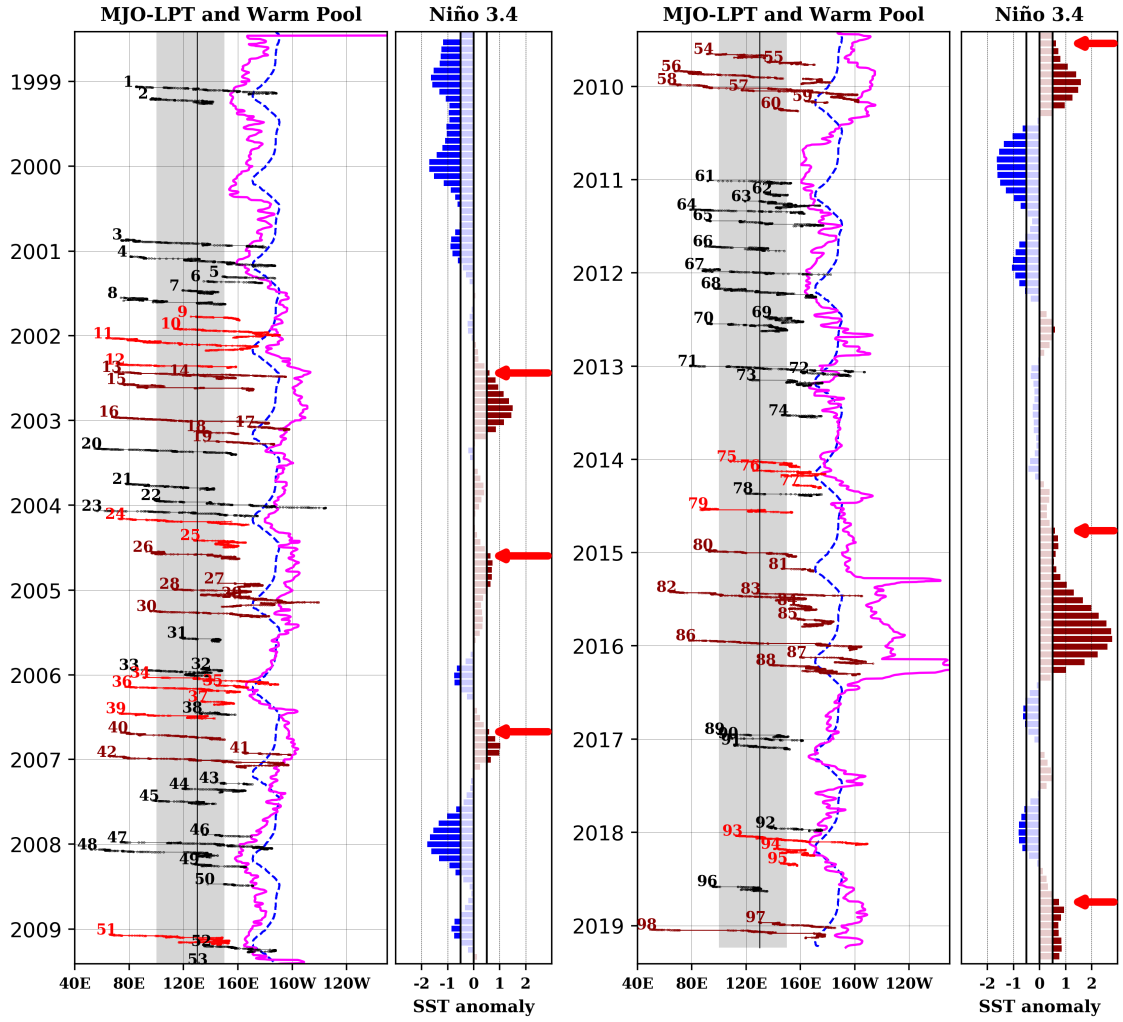

Figure 3.3: The EqWP in magenta and its climatology in blue. The 3-months centered Niño 3.4 in horizontal bars, highlighted for anomalies above (below) 0.5°C (-0.5°C) in dark-red (blue). The onset of El Niño events (red arrows) corresponds to Niño 3.4 above 0.5°C for five consecutive overlapping three-month seasons for the first time. MJO events highlighted in red if they occurred within 9 months prior to the onset of El Niño only if they are associated with a WPEE. MJO events highlighted in dark-red correspond to events during El Niño, the rest are non-El Niño related are in black.

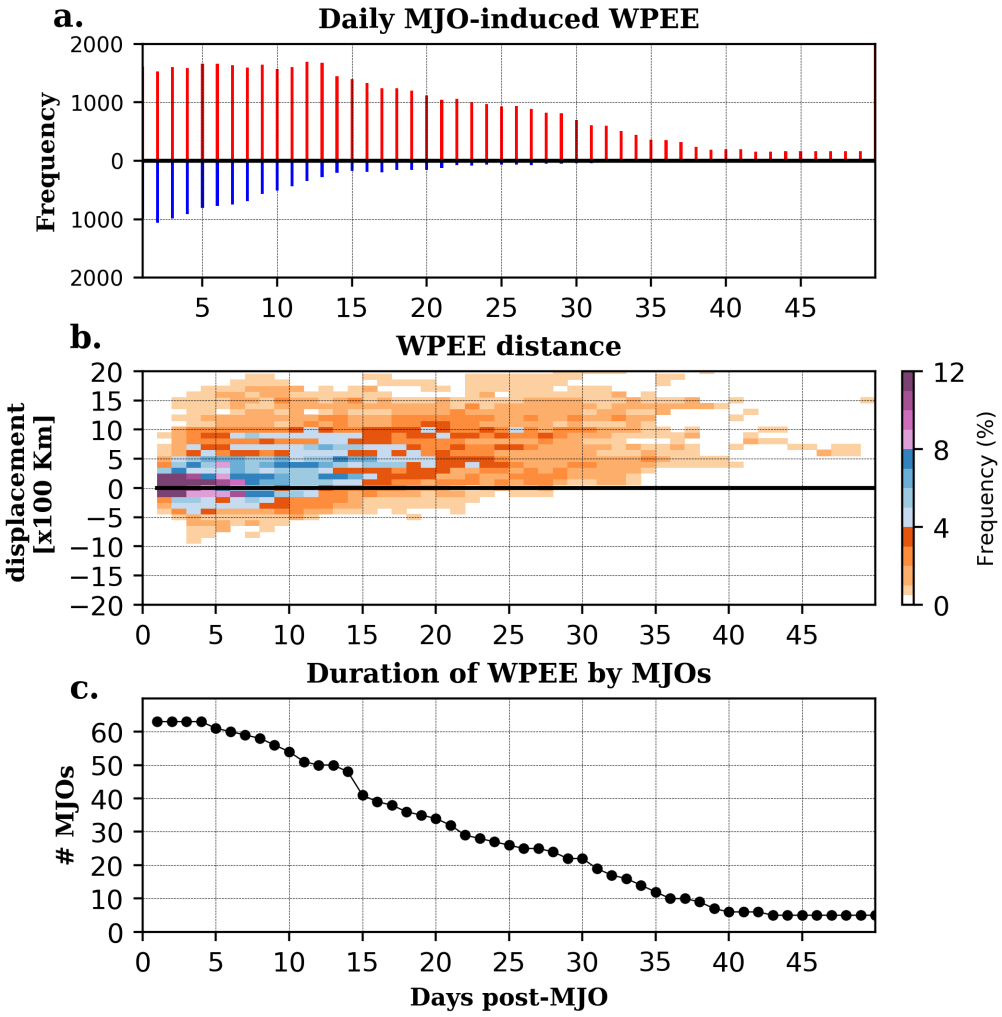

Figure 3.4: Characteristics of the MJO-induced WPEE as a function of days post-MJO precipitation. (a) frequency of displacement in number per day, and (b) histogram of the WPEE displacement (in km), within 1-degree bin in y-axis, and (c) number of the MJO that produced WPEE.

EqWP ending longitude and the same Day-Max, which indicates a continuous WPEE associated with these MJO events. We found six cases, three occurred before El Niño onset (24-25, 34-36, and 93-96), two during El Niño 2009/10 (54-55, 57-59) and only one (1-2) during La Niña 1999.

The MJO events with significant impact on the WPEE often occur during boreal, these

events can sustain displacements up to 3,000 *km* (Figure 3.6a and b). These results are consistent with previous studies [51, 26] that identified boreal spring as the time when the growth of ENSO SST anomalies is most sensitive to MJO forcing. Spring is characterized with relatively weak horizontal SST gradients and trade winds; thus, small perturbations can be amplified by unstable air-sea interactions over a larger domain [35, 52, 24, 23, 17]. According to these arguments, if MJO activity is elevated during spring, the WPEE leads to strong basin-wide warm SST anomalies in the Pacific [47] leading to the development of El Niño the following boreal winter as was demonstrated with robust lagged-correlations by [26].

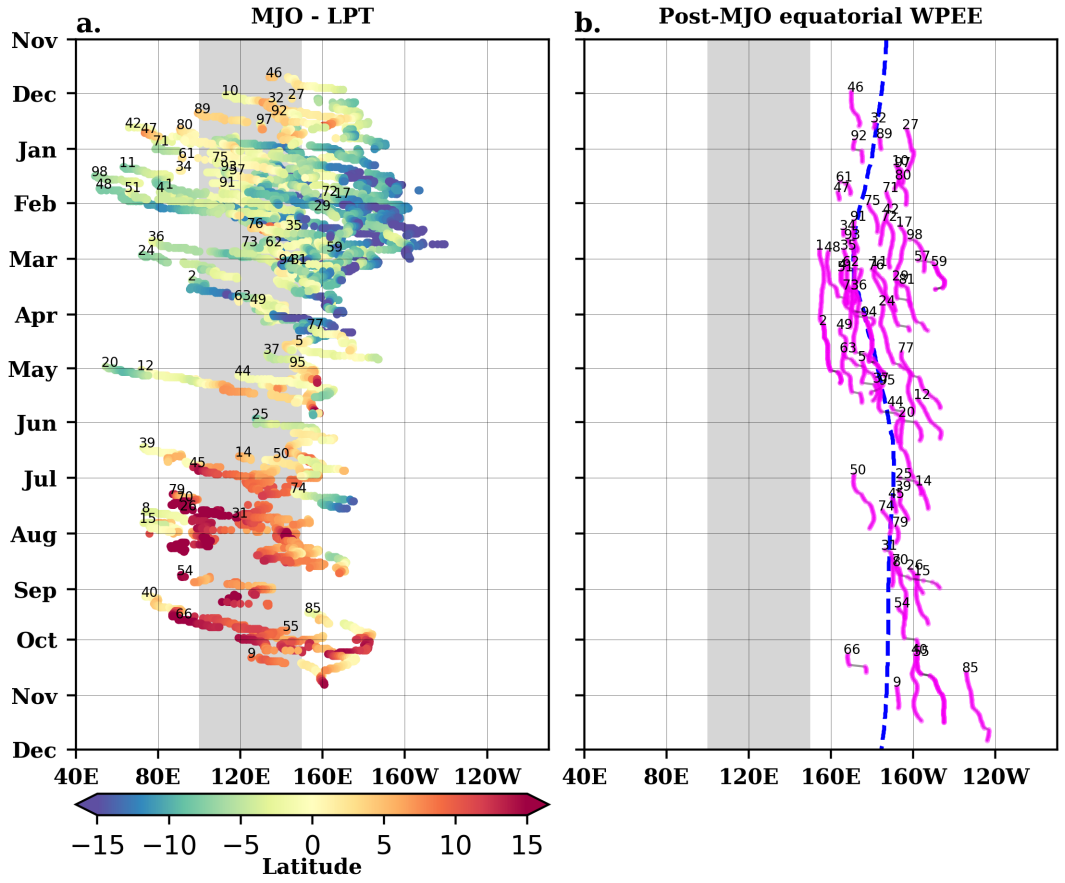

Figure 3.5: (a) Number of MJO events occurred before the onset of El Niño events from 1998 - 2019 by season. (b) The Max-WPEE associated with each MJO event shown in panel (a), by season. Seasons: DJF (December to February), MAM (March to May), JJA (June to August), SON (September to November).

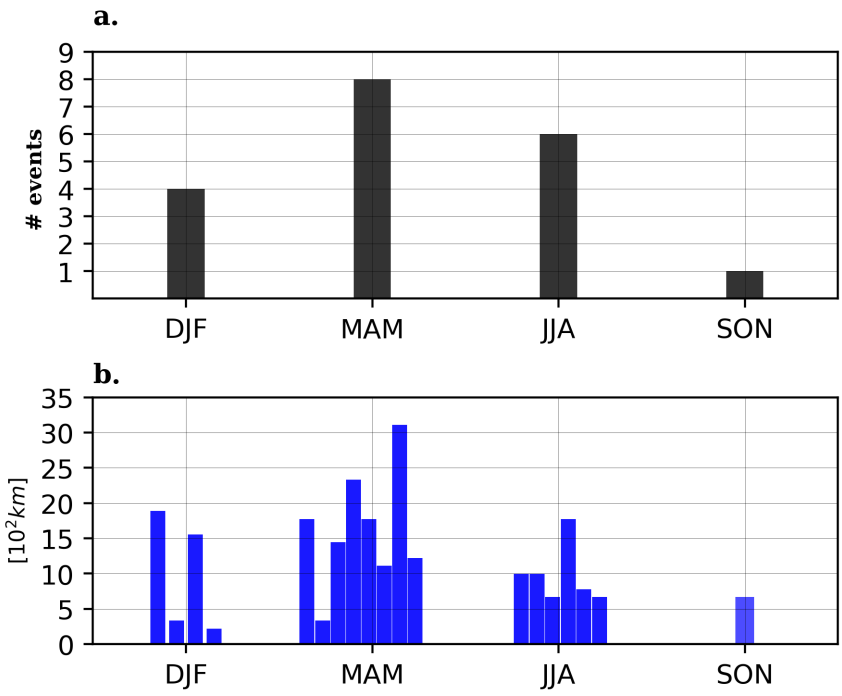

Figure 3.6: (a)MJO-LPT centroids for the 63 MJO that are associated with a post-event WPEE, colors indicate latitude and they are numbered by their id. (b) The equatorial WPEE post-MJO events in panel (a) Dashed blue line indicates the EqWP daily climatology.

3.3.2 MJO-induced WPEE anomaly

The local and remote impacts of the MJO on the Pacific SST depend to a first approximation, on its position in the western Pacific relative to the warm pool eastern edge. We hypothesize that a larger MJO zonal fetch that reaches the vicinity of the warm pool edge induces a larger WPEE. Similarly, an off-equatorially MJO propagating feature, far away from the warm pool edge, might have a less direct impact on the WPEE. To test this idea, we compare the MJO propagation extent and the WPEE within each group identified in Section 4. Top panels in Figure 3.8 show the MJO-LPT centroids for each event within each group, non-El Niño, before El Niño and during El Niño. The initial and ending location provides the zonal MJO propagation extent. Lower panels show the Confidence Intervals (CI) at 95% significance (z = 1.96) computed using the WPA at Day-0 (D0) and Day-Max

(Dmax). The thick blue and red lines are the averages for each group at D0 and Dmax. The distance between these averages provides the WPEE anomalous displacement per latitude from 10°S to 10°N, each 0.25°. These results indicate that the anomalous WPEE is a robust signal, especially in the equatorial region but pronounced in the northern hemisphere. The non-El Niño related group is associated with a relatively short displacement (1,000km). However, the group that includes events before the El Niño onset induced larger anomalous WPEE (2,000km), especially from 5°S to 10°N. Besides, these events started with a WPA anomaly of about 500km at 5°N (Figure 13b), which indicates that the WPEE began during the MJO events. In contrast, during El Niño events, the warm pool is already in an unusual eastern position. Still, the MJO events induce a further eastward anomalous WPEE (Figure 13c).

The MJO impact on the warm pool is more pronounced on the north tropical hemisphere (up to 10°N), especially for the before El Niño onset group and during the El Niño group (Figure 13b and c). One possible explanation comes from the large spatial variability of the warm pool (Figure 2.5) and the ending centroid location of the MJO events. Given that MJO events propagate mostly in the equatorial region wobbling between 10°S to 10°N, they most likely impact the warm pool in the northern hemisphere during winter and spring. Still, they have less impact on the southern hemisphere. Most of the MJO events for the non-El Niño group occur during boreal winter when the warm pool is too far east located (Figure 2.5). In contrast, the MJO impact on the WPEE for the before El Niño onset group often occurs in boreal spring (Figure 3.7) when the warm pool is on its westernmost location.

3.4 MJO intensity in relation to the WPEE

This section uses the MJO intensity as a metric to compare individual and consecutive MJO events in relation to the WPEE. Events during El Niño conditions (33 events highlighted in dark red in Figure 3) are excluded to ensure that the WPEE comes from MJO events and not from underlying El Niño conditions. We examine a total of 46 WPEE events and 19 events associated with a warm pool westward displacement. Events that occurred before

the onset of El Niño events are highlighted in red squares, and the rest are shown in gray circles in Figure 14a, b, and c.

The MJO intensity in terms of rain volume varies from 0.03 to 1.5km^3 with a mean of 0.5km^3, and in terms of WWBs varies from 0.17 to 4.2ms^{-1} with a mean of 1.6ms^{-1}. Generally, the WPEE associated with individual events increases with the amount of rainfall and intensity of WWB (Figure 13a and b). Most MJO events before the El Niño onset are characterized with large rain volume and strong WWBs, and they are associated with significant WPEE (Figure 14c). However, the fact that some strong MJO events are associated with warm pool westward displacement and the large spread between MJO intensity and WPEE suggest that (i) each MJO event is different (e.g., duration, structure, and intensity) and (ii) each MJO impact the warm pool differently. Besides, the impact of a given MJO on the ocean state depends on the initial state of the ocean [7].

Consecutive MJO events can affect the ocean state on long timescales, as demonstrated by previous studies [32, 7]. To examine the net impact of consecutive MJO events on the

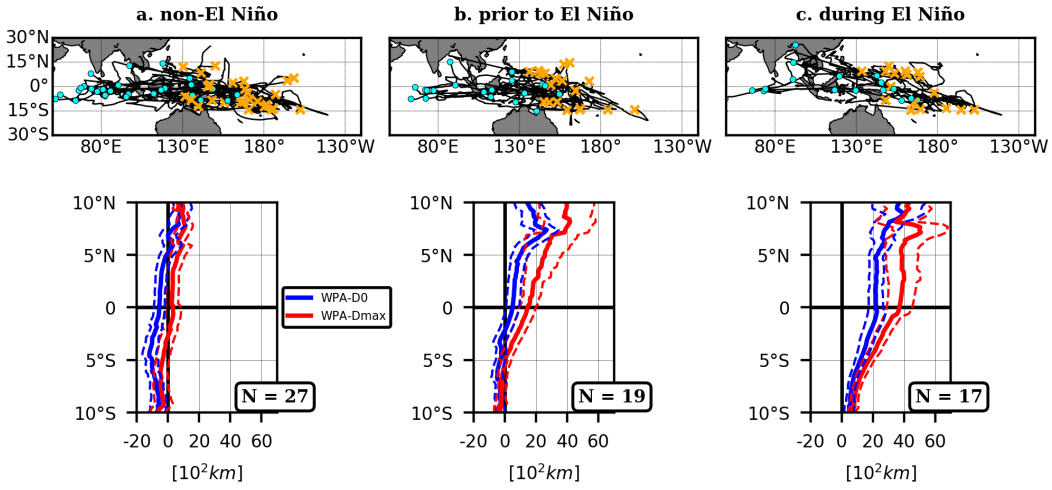

Figure 3.7: The upper panel show the initial (cyan) and ending(orange) MJO-centroids for (a) 27 MJO events that are non-El Niño related, (b) 19 MJOs occurred prior to the onset of the El Niño, and (c) 17 MJOs during the El Niño. Dashed lines in the lower panels show the confidence intervals ($\alpha = 0.05$) of the warm pool anomaly (WPA) at Day-0 (D0, blue) and at Day-max (Dmax, red) from 10°S to 10°N. Thick lines are the mean.

WPEE, we quantitatively measure the strength of consecutive MJO events. There are two type of consecutive MJO events. One group accounts events associated with one continuous WPEE (1-2, circled marker). Another group accounts events that occurred before the onset of El Niño but not necessarily associated with a continuous WPEE (9-12, 24-25, 34-39,

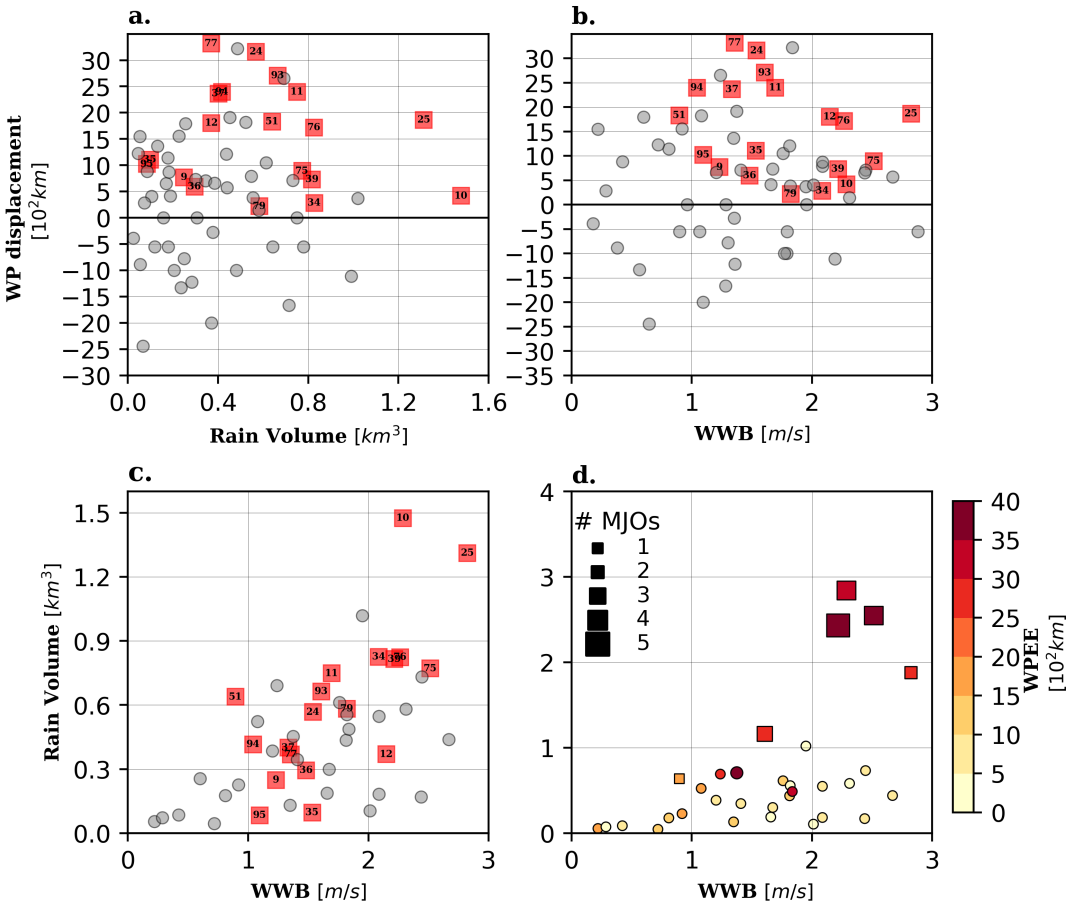

Figure 3.8: **MJO events during El Niño are excluded in all panels. MJO events highlighted in red squares occurred before the El Niño onset, and gray circled markers are the rest**. Scatter plots of the post-MJO warm pool displacement against (a) Rain Volume (km^3), and (b) WWB (ms^{-1}). Scatter plots of WWB against Rain volume for (c) individual events with WPEE and (d) grouped events color coded by eastward displacement in km. There are 6 groups of consecutive MJO events before the onset of each El Niño, the marker size indicate the number of MJO event within a group. The Rain volume for each group correspond to the cumulative rainfall from consecutive MJO events, and WWB correspond to the maximum WWB within the group.

51, 75-79, 93-95, squared markers). The Rain Volume representative of the group is the accumulated Rain Volume of individual events, and the WWB corresponds to the maximum within the group. Grouped MJOs Rain Volume and WWB are shown in Figure 14d colored by the total WPEE and with marker sizes proportional to the number of events. The total WPEE is quantified as the accumulation of individual displacements. As expected, larger WPEE is associated with consecutive MJO events with strong WWBs and large accumulated Rain Volume, especially before the onset of El Niño. Only one MJO event (51) associated with a WPEE of about 1,500 km is observed before El Niño 2009/10. The rest of El Niño events were preceded by 3 to 5 MJO events within 9 months before their onset. These grouped MJO events are associated with significant WPEE varying from 2,500 to 4,000km. These results support the premise that the MJO group effort has a more significant impact on the WPEE. Indeed, large WPEE associated with consecutive MJO events is the result of the long-term effect of MJO forcing on the upper ocean, and is commonly observed as large-scale SST anomalies in the equatorial Pacific Ocean that often produce large-scale wind anomalies (Figure 3.2), that under favorable can allow further growth of coupled atmosphere-ocean processes allowing the warm pool to shift further east during the onset of El Niño.

3.5 MJO-induced SST anomalies composites

The occurrence of WWBs has been used to explore the predictability of the tropical Pacific climate [36] and 50% of the variance of zonal winds in the west Pacific come from intraseasonal variability [26]. Indeed, the MJO plays a particular role as one of the main contributors since it affects the surface fluxes coherently over thousands of kilometers near the equator [42], during and after the convective signal [32, 7]. The precise mechanism by which intraseasonal variations may rectify into lower-frequency dynamics has been the subject of several studies, all of which involve some form of SST feedback to the atmosphere. This section explores the net MJO effect on SST anomalies obtained from composite maps during and after the MJO signal in the western Pacific.

Composites of Rain volume and WWBs along the MJO-LPT propagation confirm that

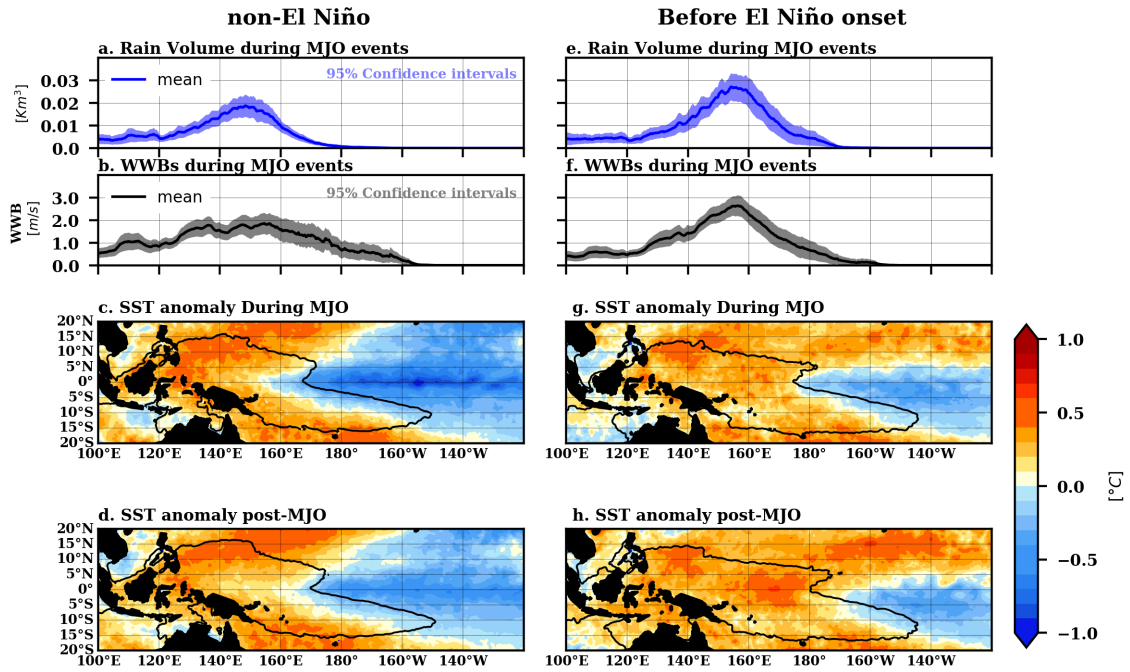

Figure 3.9: Panels a-d show composites of 27 non-El Niño related events, and panels e-h show composites of 19 MJO events occurred prior to the onset of the El Niño. Blue and gray shading show the 95% Confidence Intervals of the accumulated Volumetric rain (km^3), and the averaged WWB (ms^{-1}) inside the MJO-LPT feature from 10°S – 10°N throughout the MJO lifetime, every 0.25° in longitude. (c) and (g) show composite maps of SST anomaly (shaded) and the warm pool (black contour) during MJO-LPT lifetime in the west Pacific. (d) and (h) show composite maps of SST anomaly (shaded) and warm pool (black contour) post-MJO events, including only days from Day-0 until Day-max for each event respectively.

events before the El Niño onset group (Figure 3.9 e and f) are considerably stronger than the non-El Niño related group (Figure 3.9 a and b). The Rain Volume and WWB are significative stronger ($\alpha = 0.05$) in 0.01 km^3 and $1ms^{-1}$, especially between 150°E - 170°E. SST anomaly composite maps during the MJO-LPT propagation illustrate two different ocean background conditions. Strong east-west SST anomalies dominate Pacific (140°E - 160°W) for the non-El Niño related group, likely associated with strong trade winds. In contrast, the El Niño onset group display weak east-west SST anomalies. These composites maps indicate that the ocean conditions are not favorably for the WPEE for the non-El

Niño related group; however, favorable conditions for the WPEE exist for the El Niño onset group.

Chapter 4

SUMMARY AND CONCLUSIONS

Using satellite-derived rain rates and SST products, we have quantified, for the first time, the time and spatial scale of the MJO-induced warm pool eastward extension (WPEE) in the equatorial region (10°S – 10N°). We have found that 65% of the MJO events observed in the western Pacific during 1998/06 – 2019/06 had a significant impact on the WPEE, varying from 100-200km up to 3,000km. The most frequent WPEE occurs during the first 15 days post-MJO events in about 1,000km, giving a 0.8ms^{-1} eastward displacement speed (Figure 3.4). Further, we demonstrated that the observed MJO-induced WPEE before the El Niño onset is sufficiently robust and maintained beyond the annual cycle, but particularly important during the transition from boreal Spring to Summer (Figure 3.6 and 3.7). The MJO intensity of convection (Rain Volume in km^3) and westerly winds bursts (WWBs in ms^{-1}) are used as a metric to compare individual and consecutive MJO events. We found that significant WPEE ($> 2,000km$) are commonly associated with strong MJO events characterized by large Rain Volume and strong WWB (Figure 3.4), especially between 150°E - 170°E (Figure 3.8). The lack of a linear correlations between the MJO intensity and WPEE, suggests that individual events have different impacts due to different initial ocean conditions as pointed out by Bergman et al., [2001]. Furthermore, the consecutive MJO impact on the ocean has long-term implications as shown by significant WPEE observed before each El Niño event in the period studied (Figure 3.8d). The MJO-induced WPEE induces large-scale warm anomalies (0.5°C) in the Central Pacific (160°E-180°E, 10°S-10°N), east of the maximum intensity of Rain and WWBs (Figure 3.9), that occurs at much shorter timescale than those associated with ENSO. The results described in this study is limited by considering only SST, winds and rainfall satellite observations. Our methodology does not allow the examination of the full coupled complexity of the phenomenon that involves oceanic equatorial waves in Pacific. However, the results should nevertheless be

useful in evaluating atmosphere-ocean coupled simulations. Reproducing the location and intensity of the MJO rain and WWBs is important to obtain a good representation of the ocean dynamics and thermodynamics response needed to the WPEE.

BIBLIOGRAPHY

[1] Steven P. Anderson, Robert A. Weller, and Roger B. Lukas. Surface Buoyancy Forcing and the Mixed Layer of the Western Pacific Warm Pool: Observations and 1D Model Results. *Journal of Climate*, 9(12):3056–3085, 1996.

[2] Robert Atlas, Joseph Ardizzone, and Ross N. Hoffman. Application of satellite surface wind data to ocean wind analysis. In Philip E. Ardanuy and Jeffery J. Puschell, editors, *Remote Sensing System Engineering*, volume 7087, pages 118 – 124. International Society for Optics and Photonics, SPIE, 2008.

[3] T P Barnett. Variations in Near-Global Sea Level Pressure. *Journal of the Atmospheric Sciences*, 42(5):478–501, 1985.

[4] David S Battisti and Anthony C Hirst. Interannual Variability in a Tropical Atmosphere–Ocean Model: Influence of the Basic State, Ocean Geometry and Nonlinearity. *Journal of the Atmospheric Sciences*, 46(12):1687–1712, 1989.

[5] David S. Battisti, Daniel J. Vimont, and Benjamin P. Kirtman. 100 Years of progress in understanding the dynamics of coupled atmosphere/ocean variability 100 Years of progress in understanding the dynamics of coupled atmosphere/ocean variability. *Meteorological Monographs*, 2019.

[6] John W. Bergman, Harry H. Hendon, and Klaus M. Weickmann. Intraseasonal Air–Sea Interactions at the Onset of El Niño. *Journal of Climate*, 14(8):1702–1719, 2001.

[7] John W. Bergman, Harry H. Hendon, and Klaus M. Weickmann. Intraseasonal Air–Sea Interactions at the Onset of El Niño. *Journal of Climate*, 14(8):1702–1719, 2001.

[8] J Bjerknes. A possible response of the atmospheric Hadley circulation to equatorial anomalies of ocean temperature. *Tellus*, 18(4):820–829, 1966.

[9] J BJERKNES. ATMOSPHERIC TELECONNECTIONS FROM THE EQUATORIAL PACIFIC 1. *Monthly Weather Review*, 97(3):163–172, 1969.

[10] Christelle Bosc, Thierry Delcroix, and Christophe Maes. Barrier layer variability in the western Pacific warm pool from 2000 to 2007. *Journal of Geophysical Research: Oceans (1978–2012)*, 114(C6), 2009.

[11] Allan J. Clarke, Jianguo Wang, and Stephen Van Gorder. A Simple Warm-Pool Displacement ENSO Model. *Journal of Physical Oceanography*, 30(7):1679–1691, 2000.

[12] Sophie Cravatte, Thierry Delcroix, Dongxiao Zhang, Michael McPhaden, and Julie Leloup. Observed freshening and warming of the western Pacific Warm Pool. *Climate Dynamics*, 33(4):565–589, 2009.

[13] Thierry Delcroix, Gerard Eldin, and Christian Hénin. Upper Ocean Water Masses and Transports in the Western Tropical Pacific (165°E). *Journal of Physical Oceanography*, 17(12):2248–2262, 1987.

[14] Thierry Delcroix and Joël Picaut. Zonal displacement of the western equatorial Pacific "fresh pool". *Journal of Geophysical Research: Oceans*, 103(C1):1087–1098, 1998.

[15] Charlotte A. DeMott, Nicholas P. Klingaman, and Steven J. Woolnough. Atmosphere-ocean coupled processes in the Madden-Julian oscillation. *Reviews of Geophysics*, 53(4):1099–1154, 2015.

[16] Clara Deser and John M Wallace. Large-Scale Atmospheric Circulation Features of Warm and Cold Episodes in the Tropical Pacific. *Journal of Climate*, 3(11):1254–1281, 1990.

[17] Ian Eisenman, Lisan Yu, and Eli Tziperman. Westerly Wind Bursts: ENSO's Tail Rather than the Dog? *Journal of Climate*, 18(24):5224–5238, 2005.

[18] Gérard Eldin, Thierry Delcroix, and Martine Rodier. The frontal area at the eastern edge of the western equatorial Pacific warm pool in April 2001. *Journal of Geophysical Research: Oceans*, 109(C7), 2004.

[19] Congbin Fu, H F Diaz, and J O Fletcher. Characteristics of the Response of Sea Surface Temperature in the Central Pacific Associated with Warm Episodes of the Southern Oscillation. *Monthly Weather Review*, 114(9):1716–1739, 1986.

[20] J S Godfrey, R A Houze, R H Johnson, R Lukas, J L Redelsperger, A Sumi, and R Weller. Coupled Ocean-Atmosphere Response Experiment (COARE): An interim report. *Journal of Geophysical Research: Oceans*, 103(C7):14395–14450, 1998.

[21] J. S. Godfrey and E. J. Lindstrom. The heat budget of the equatorial western Pacific surface mixed layer. *Journal of Geophysical Research: Oceans*, 94(C6):8007–8017, 1989.

[22] N E Graham and T P Barnett. Sea Surface Temperature, Surface Wind Divergence, and Convection over Tropical Oceans. *Science*, 238(4827):657–659, 1987.

[23] D E Harrison and Benjamin S Giese. Episodes of surface westerly winds as observed from islands in the western tropical Pacific. *Journal of Geophysical Research*, 96(S01):3221, 1991.

[24] D E Harrison and Paul S Schopf. Kelvin-Wave-Induced Anomalous Advection and the Onset of Surface Warming in El Niño Events. *Monthly Weather Review*, 112(5):923–933, 1984.

[25] Harry H. Hendon, Matthew C. Wheeler, and Chidong Zhang. Seasonal Dependence of the MJO–ENSO Relationship. *Journal of Climate*, 20(3):531–543, 2007.

[26] Harry H. Hendon, Matthew C. Wheeler, and Chidong Zhang. Seasonal Dependence of the MJO–ENSO Relationship. *Journal of Climate*, 20(3):531–543, 2007.

[27] Harry H. Hendon, Chidong Zhang, and John D. Glick. Interannual Variation of the Madden–Julian Oscillation during Austral Summer. *Journal of Climate*, 12(8):2538–2550, 1999.

[28] George J Huffman, David T Bolvin, Eric J Nelkin, David B Wolff, Robert F Adler, Guojun Gu, Yang Hong, Kenneth P Bowman, and Erich F Stocker. The TRMM Multisatellite Precipitation Analysis (TMPA): Quasi-Global, Multiyear, Combined-Sensor Precipitation Estimates at Fine Scales. *Journal of Hydrometeorology*, 8(1):38–55, 2007.

[29] Yakelyn R. Jauregui and Ken Takahashi. Simple physical-empirical model of the precipitation distribution based on a tropical sea surface temperature threshold and the effects of climate change. *Climate Dynamics*, 50(5-6):2217–2237, 2018.

[30] Brandon W. Kerns and Shuyi S. Chen. Large-scale precipitation tracking and the MJO over the Maritime Continent and Indo-Pacific warm pool. *Journal of Geophysical Research: Atmospheres*, 121(15):8755–8776, 2016.

[31] William S. Kessler. Is ENSO a cycle or a series of events? *Geophysical Research Letters*, 29(23):40–1–40–4, 2002.

[32] William S. Kessler and Richard Kleeman. Rectification of the Madden–Julian Oscillation into the ENSO Cycle. *Journal of Climate*, 13(20):3560–3575, 2000.

[33] William S Kessler, Michael J McPhaden, and Klaus M Weickmann. Forcing of intraseasonal Kelvin waves in the equatorial Pacific. *Journal of Geophysical Research*, 100(C6):10613, 1995.

[34] Jong-Seong Kug, K.-P. Sooraj, Tim Li, and Fei-Fei Jin. Precursors of the El Niño/La Niña onset and their interrelationship. *Journal of Geophysical Research: Atmospheres (1984–2012)*, 115(D5), 2010.

[35] M Latif, T P Barnett, M A Cane, M Flügel, N E Graham, H von Storch, J S Xu, and S E Zebiak. A review of ENSO prediction studies. *Climate Dynamics*, 9(4-5):167–179, 1994.

[36] Mojib Latif and Moritz Flügel. An investigation of short-range climate predictability in the tropical Pacific. *Journal of Geophysical Research: Oceans*, 96(C2):2661–2673, 1991.

[37] Matthieu Lengaigne, Jean-Philippe Boulanger, Christophe Menkes, Gurvan Madec, Pascale Delecluse, Eric Guilyardi, and Julia Slingo. The March 1997 Westerly Wind Event and the Onset of the 1997/98 El Niño: Understanding the Role of the Atmospheric Response. *Journal of Climate*, 16(20):3330–3343, 2003.

[38] Matthieu Lengaigne, Jean-Philippe Boulanger, Christophe Menkes, Sebastien Masson, Gurvan Madec, and Pascale Delecluse. Ocean response to the March 1997 Westerly Wind Event. *Journal of Geophysical Research: Oceans (1978–2012)*, 107(C12):SRF 16–1–SRF 16–20, 2002.

[39] Roger Lukas and Eric Lindstrom. The mixed layer of the western equatorial Pacific Ocean. *Journal of Geophysical Research: Oceans*, 96(S01):3343–3357, 1991.

[40] Roland A Madden and Paul R Julian. Detection of a 40–50 Day Oscillation in the Zonal Wind in the Tropical Pacific. *Journal of the Atmospheric Sciences*, 28(5):702–708, 1971.

[41] Roland A Madden and Paul R Julian. Description of Global-Scale Circulation Cells in the Tropics with a 40–50 Day Period. *Journal of the Atmospheric Sciences*, 29(6):1109–1123, 1972.

[42] Roland A. Madden and Paul R. Julian. Observations of the 40–50-Day Tropical Oscillation—A Review. *Monthly Weather Review*, 122(5):814–837, 1994.

[43] Christophe Maes, Michael J. McPhaden, and David Behringer. Signatures of salinity variability in tropical Pacific Ocean dynamic height anomalies. *Journal of Geophysical Research: Oceans (1978–2012)*, 107(C12):SRF 13–1–SRF 13–13, 2002.

[44] Christophe Maes, Joël Picaut, Yoshifumi Kuroda, and Kentaro Ando. Characteristics of the convergence zone at the eastern edge of the Pacific warm pool. *Geophysical Research Letters*, 31(11):n/a–n/a, 6 2004.

[45] A. G. Marshall, O. Alves, and H. H. Hendon. A Coupled GCM Analysis of MJO Activity at the Onset of El Niño. *Journal of the Atmospheric Sciences*, 66(4):966–983, 2009.

[46] M. J. McPhaden and J. Picaut. El Niño-Southern Oscillation Displacements of the Western Equatorial Pacific Warm Pool. *Science*, 250(4986):1385–1388, 1990.

[47] M J McPhaden, S E Zebiak, and M H Glantz. ENSO as an Integrating Concept in Earth Science. *Science*, 314(5806):1740–1745, 2006.

[48] Michael J. McPhaden. Genesis and Evolution of the 1997-98 El Niño. *Science*, 283(5404):950–954, 1999.

[49] Michael J McPhaden. Mixed Layer Temperature Balance on Intraseasonal Timescales in the Equatorial Pacific Ocean*. *Journal of Climate*, 15(18):2632–2647, 2002.

[50] Michael J. McPhaden and Xuri Yu. Equatorial waves and the 1997–98 El Niño. *Geophysical Research Letters*, 26(19):2961–2964, 1999.

[51] Andrew M. Moore and Richard Kleeman. Stochastic Forcing of ENSO by the Intraseasonal Oscillation. *Journal of Climate*, 12(5):1199–1220, 1999.

[52] S. G. H. Philander, T. Yamagata, and R. C. Pacanowski. Unstable air-sea interactions in the tropics. *Journal of the Atmospheric Sciences*, 41(4):604–613, 1984.

[53] J. Picaut, F. Masia, and Y. du Penhoat. An Advective-Reflective Conceptual Model for the Oscillatory Nature of the ENSO. *Science*, 277(5326):663–666, 1997.

[54] Joel Picaut, Mansour Ioualalen, Thierry Delcroix, François Masia, Ragu Murtugudde, and Jérome Vialard. The oceanic zone of convergence on the eastern edge of the Pacific warm pool: A synthesis of results and implications for El Niño-Southern Oscillation and biogeochemical phenomena. *Journal of Geophysical Research: Oceans*, 106(C2):2363–2386, 2001.

[55] Joël Picaut and Thierry Delcroix. Equatorial wave sequence associated with warm pool displacements during the 1986–1989 El Niño-La Niña. *Journal of Geophysical Research: Oceans*, 100(C9):18393–18408, 1995.

[56] Eugene M Rasmusson and Thomas H Carpenter. Variations in Tropical Sea Surface Temperature and Surface Wind Fields Associated with the Southern Oscillation/El Niño. *Monthly Weather Review*, 110(5):354–384, 1982.

[57] Richard W. Reynolds, Nick A. Rayner, Thomas M. Smith, Diane C. Stokes, and Wanqiu Wang. An Improved In Situ and Satellite SST Analysis for Climate. *Journal of Climate*, 15(13):1609–1625, 2002.

[58] Richard W Reynolds, Thomas M Smith, Chunying Liu, Dudley B Chelton, Kenneth S Casey, and Michael G Schlax. Daily High-Resolution-Blended Analyses for Sea Surface Temperature. *Journal of Climate*, 20(22):5473–5496, 2007.

[59] C F Ropelewski and M S Halpert. Precipitation Patterns Associated with the High Index Phase of the Southern Oscillation. *Journal of Climate*, 2(3):268–284, 1989.

[60] Paul S Schopf and Max J Suarez. Ocean Wave Dynamics and the Time Scale of ENSO. *Journal of Physical Oceanography*, 20(5):629–645, 1990.

[61] Simon P. de Szoeke, James B. Edson, June R. Marion, Christopher W. Fairall, and Ludovic Bariteau. The MJO and Air–Sea Interaction in TOGA COARE and DYNAMO. *Journal of Climate*, 28(2):597–622, 2015.

[62] Jérôme Vialard and Pascale Delecluse. An OGCM Study for the TOGA Decade. Part II: Barrier-Layer Formation and Variability. *Journal of Physical Oceanography*, 28(6):1089–1106, 1998.

[63] B. Wang. Transition from a cold to a warm state of the El Niño-Southern Oscillation cycle. *Meteorology and Atmospheric Physics*, 56(1-2):17–32, 1995.

[64] Bin Wang and Tianming Li. Convective Interaction with Boundary-Layer Dynamics in the Development of a Tropical Intraseasonal System. *Journal of the Atmospheric Sciences*, 51(11):1386–1400, 1994.

[65] Chunzai Wang and David B. Enfield. The tropical western hemisphere warm pool. *Geophysical Research Letters*, 28(8):1635–1638, 2001.

[66] Chunzai Wang and JoëL Picaut. Geophysical Monograph Series. pages 21–48, 2004.

[67] Peter J. Webster and Roger Lukas. Toga coare: The coupled ocean–atmosphere response experiment. *Bulletin of the American Meteorological Society*, 73(9):1377–1416, 1992.

[68] Klaus Wyrtki. Water displacements in the Pacific and the genesis of El Nino cycles. *Journal of Geophysical Research*, 90(C4):7129, 1985.

[69] Kozo Yoshida. A Theory of the Cromwell Current (the Equatorial Undercurrent) and of the Equatorial Upwelling. *Journal of the Oceanographical Society of Japan*, 15(4):159–170, 1959.

[70] Lisan Yu, Robert A. Weller, and W. Timothy Liu. Case analysis of a role of ENSO in regulating the generation of westerly wind bursts in the Western Equatorial Pacific. *Journal of Geophysical Research: Oceans (1978–2012)*, 108(C4), 2003.

[71] Chidong Zhang. Madden-Julian Oscillation. *Reviews of Geophysics*, 43(2), 2005.

[72] Chidong Zhang and Jonathan Gottschalck. SST Anomalies of ENSO and the Madden–Julian Oscillation in the Equatorial Pacific*. *Journal of Climate*, 15(17):2429–2445, 2002.